Polymer indentation with mesoscopic molecular dynamics

Javier R. Rocha, Kevin Z. Yang, Travis Hilbig, and Witold Brostow[a)]
Laboratory of Advanced Polymers and Optimized Materials (LAPOM), Department of Materials Science and Engineering and Department of Physics, University of North Texas, Denton, Texas 76207

Ricardo Simoes
School of Technology, Polytechnic Institute of Cávado and Ave, Campus do IPCA, 4750-810 Barcelos, Portugal; and Institute for Polymers and Composites - IPC/I3N, University of Minho, Campus de Azurem, 4800-058 Guimaraes, Portugal

(Received 22 July 2013; accepted 18 September 2013)

Indentation tests are used to determine the hardness of a material, e.g., Rockwell, Vickers, or Knoop. The indentation process is empirically observed in the laboratory during these tests; the mechanics of indentation is insufficiently understood. We have performed first molecular dynamics computer simulations of indentation resistance of polymers with a chain structure similar to that of high density polyethylene (HDPE). A coarse grain model of HDPE is used to simulate how the interconnected segments respond to an external force imposed by an indenter. Results include the time-dependent measurement of penetration depth, recovery depth, and recovery percentage, with respect to indenter force, indenter size, and indentation time parameters. The simulations provide results that are inaccessible experimentally, including continuous evolution of the pertinent tribological parameters during the entire indentation process.

I. INTRODUCTION

Indentation experiments are used to measure the hardness of materials and have the basic goal of quantifying material's resistance to plastic deformation. The Vickers hardness test is commonly used due to its wide range of scale capabilities to measure the hardness of metallic and ceramic materials but has only recently been used for characterizing polymers such as polymethyl methacrylate and high-density polyethylene (HDPE).[1] The Knoop hardness test is usually performed in the microindentation of very brittle materials or thin sheets. Indentation tests are related to mechanical properties such as Young's modulus, elastic moduli, yield strength, strain-hardening characteristics, residual stresses, and fracture toughness.[2,3] These tests can also be used to measure the strength of polymer coatings and the interface between the coating and the substrate.[4]

During the past three decades, the range of indentation testing has been extended down to the nanometer range through the development of instruments capable of continuously measuring load and displacement throughout the indentation process. Applications in the nanoindentation range include the characterization of the viscoelastic behavior of hierarchical structures such as bone and other biomaterials.[5,6] The majority of nanoindentation tests measure the properties of metals and hard thin films for microelectronic applications.[7–9] A smaller subset of nanoindentation studies involve polymeric materials, some of which include quasi-static and dynamic nanoindentation of HDPE.[10–13] Conventionally, nanoindentation and atomic force microscopy (AFM) can be used to generate values for the relative elastic moduli of polymer blends. AFM has been used to measure nanomechanical properties and identify the phases in blends of linear HDPE.[14]

Computer simulations are becoming an increasingly practical tool and provide many advantages over experimental research. The simulations allow us to determine properties that are difficult or impossible to measure experimentally. Moreover, one can produce a large quantity of results very rapidly. Still further, we can fully control the parameters in the system, and the variables can be determined simultaneously with high accuracy.[15] Simulations allow us to handle a variety of experimental conditions, namely at the very small or large scale that may otherwise be difficult to test experimentally. Links between computational studies and experimental techniques are sometimes provided; e.g., Cleymand et al.[16] used a simulation to confirm the results of nanoindentation experiments on thin films and showed that the elastic response of bilayer materials is specific to a particular coating for low indentation depths. Despite the benefits present in computational simulations, compared to experimental research, simulations represent a very small percentage of the literature.

We base our simulations on the molecular dynamics (MD) method, originally developed by Alder and Wainwright.[17] MD is conceptually simple: we apply Newton's second law ($F = m \times a$, with symbols widely

[a)]Address all correspondence to this author.
e-mail: wbrostow@yahoo.com
DOI: 10.1557/jmr.2013.307

used) to a many-body system over a number of very short time intervals. Applications in polymer MD include crystallization in melts,[18] the effect of load and chain length,[19] stress relaxation for chains in dense polymeric systems,[20] and segmental mobility of polyethylene.[21] Technical details of the MD method applied to polymeric materials have been provided by several authors.[15,22–27]

Literature shows that MD simulations of nanoindentation have been applied primarily to metallic materials.[28–34] This is understandable, given the crystalline structure inherent in metals and the ease of computationally creating a monoatomic lattice. Polymeric materials, on the other hand, with short and long chains that interweave between one another, make application of the MD technique much more challenging. Simulations of polymers are more complicated since they involve inclusion of connectedness of particles (polymer chain segments), not needed when dealing with atoms or ions.

Unlike metals and ceramics, polymeric materials exhibit viscoelastic behavior, i.e., after a polymer is indented or otherwise deformed, it recovers a portion of the deformation. Viscoelastic materials are materials that have both the elastic and viscous properties. Elastic materials quickly recover the original size and shape, once the stress is removed, whereas viscous materials strain along with the stress. Ceramics typically do not exhibit measurable viscoelasticity, whereas metals show small such effects.

In microindentation experiments, two values are measured: the penetration depth, R_p, and the residual (healing or recovery) depth, R_h. R_p is the instantaneous depth that the indenter reaches at a specific location and time. R_h is the final depth that the material recovers to after the indentation process. Both of these values are explained more in the following section.

Other than measuring R_p and R_h, the only other methods of analysis for experimental indentation is imaging from optical microscopes, or in the case of nanometer scale indentation, a scanning electron microscope (SEM). SEM observations give us only the material status before and after indentation. Simulations allow us to observe the time-dependent behavior of material response as well as to quantify penetration and recovery trends.

II. SIMULATION MODEL AND METHOD

As mentioned, we use MD to determine the evolution of the interaction of particles over time by numerically solving Newton's second law. Particles can be atoms, ions, molecules, or polymer chain segments. A set of interaction potentials is used to model the response of pairwise interactions and solved for the entire system, namely,

$$m_i(d^2/dt^2)\mathbf{r}_i(t) = -\nabla U(\mathbf{r}_i), i = 1, 2, 3, \&, \ldots, N \quad , \quad (1)$$

where $U(\mathbf{r}_i)$ is the total potential energy between particles i with mass m_i and position $\mathbf{r}_i$ at time t. In our case, we have used a computer model of HDPE using the statistical segment approach espoused by Flory,[26] with each segment representing roughly two hundred C_2H_4 monomeric units. This is usually called a course-grain[35] model and is used to increase the time and length scales accessible within reasonable computational resources.[36] The interaction potentials are based on Mie (often called Lennard Jones) potentials and have been described in more detail in previous papers.[24,25] In short, the segments have an optimal distance from each other; there is a steeply increasing repulsive force when segments move close to one another and a growing weaker attractive force when they move away from one another. As described in detail in an earlier paper,[37] material generation begins by placing segments on a triangular lattice in a 3D space. Each position then represents a chain with a length of one segment. We form a bond between the two ends of neighboring chains that are the closest together. Since in the beginning all the segments are equidistant, a random number generator is used to determine which segments are bonded. This procedure is continued until no more chains of length two can be created. We then form chains of longer lengths until there are no more neighboring segments at the ends of chains that can be bonded. Thus, the result is a set of randomly coiled nonintersecting chains, with segments on triangular lattice positions, and some vacancies.

Before the indentation process, the material is allowed to equilibrate with no external forces acting. Essentially, the segments are left to interact with each other based on the intersegment and intrasegment interaction potentials. The intrapotential distance is 1.6 times the distance of the interpotential distance. We allow the material to equilibrate for 50 simulation steps. Each simulation step represents 2000 time steps, or 10 ns, meaning that the equilibration equals 0.5 μs. After each time step, segment positions are recalculated. Before equilibration, the segment positions are based on the triangular lattice, where the initial chains are formed, but since intra- and intersegmental equilibrium distances are somewhat different, the lattice positions do not provide a minimum energy configuration. Naturally, the segments are not uniformly spaced after equilibration. Thus, the equilibrium process is necessary so that the material is in a stable state before we add external forces. We perform this equilibration until the segment positions change no more than 1%, a value we have previously used to define full recovery[37] after each simulation step. The model and method used here have been explained earlier.[25,37–39]

During simulation, an indenter is applied to the center of the top surface of the material. For simplicity, we use a "good" indenter: it does not have any reactions with HDPE. It is simply modeled as an external force applied onto the material. The indentation force is aligned perpendicularly to the surface for a user-defined number of

simulation steps. We vary the size of the indenter by the number of segments that exhibit the external force, and the force is divided evenly among all of the segments. A round shape is assumed for the indenter (what defines which segments are selected for applying the force).

After the indentation process has been completed, the indenter is removed. The recovery after indentation is an important process as can be seen from experiments on viscoelastic materials.[40–43]

A bounding box model is used for these simulations; to not let the material flatten during simulation, we do not let the outside segments move past the box boundaries. By using this method, our materials have a constant volume, as opposed to other methods of bounding commonly used in small-scale MD simulation studies. Our bounding box method has been explained in more detail in previous work.[24]

The range of force, indenter size, and time during which the external force is applied is summarized in Table I. The external forces should not cause the indenter to penetrate the material close to the bottom layer as this would produce faulty data. Thus, forces are varied from 0.10 to 0.90 nN. The indenter size ranges from a diameter of three statistical segments, 147 nm, to seven segments, 343 nm. The time during which the external force is applied ranges from 10 to 300 ns.

The penetration depth is considered as the difference between the average depth of all the segments subjected to the external force and the average of all of the segments on the top row of the material, all measurements being taken from the center of the segments. The max penetration depth R_p is taken as the maximum average depth of the segments subjected to the external force. The recovery depth R_h is taken as the average depth of all the segments subjected to the force after sufficiently long time. In the present study, R_h was determined at 60 simulation steps after the indenter leaves the material. The recovery percentage, φ, is obtained from the two previously named parameters as:

$$\varphi = [(R_p - R_h)/R_p] \times 100 \quad . \tag{2}$$

TABLE I. Summary of simulation parameters.

Material size	600 × 600 × 600 nm
Indentation force	0.10–0.90 nN
Indenter diameter	147–343 nm
Time of applied force	10–300 ns

III. SELECTED RESULTS

Three simulation parameters are important: the applied external force, the indenter diameter, and the amount of time that the indenter is allowed to penetrate the material. We vary these parameters one at a time.

All the results shown are the average of three unique materials created with the exact same material creation parameters; due to the random nature of the chain formation mechanism, this will result in different amorphous chain spatial arrangements. The random nature of the chain configurations was also studied: thirteen materials, each of same size, were found to have on average 109.9 chains with a standard deviation of 5.2 chains. Figure 1 shows two materials with different chain structures, with each chain represented in a different color.

Figure 2 shows the visualization of the material before, during, and after indentation. The segments affected by the indenter are shown in red. During each simulation step, the positions of each segment are recorded for analysis.

A. Effects of force and indenter size

From here on, we graphically show the indentation behavior in the following way: each curve represents

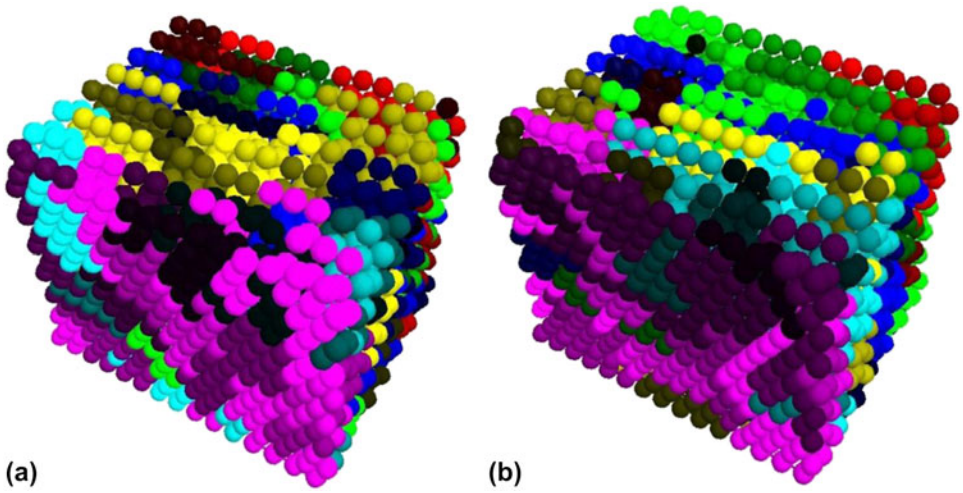

FIG. 1. Two materials with different chain structures: (a) 100 chains and (b) 118 chains.

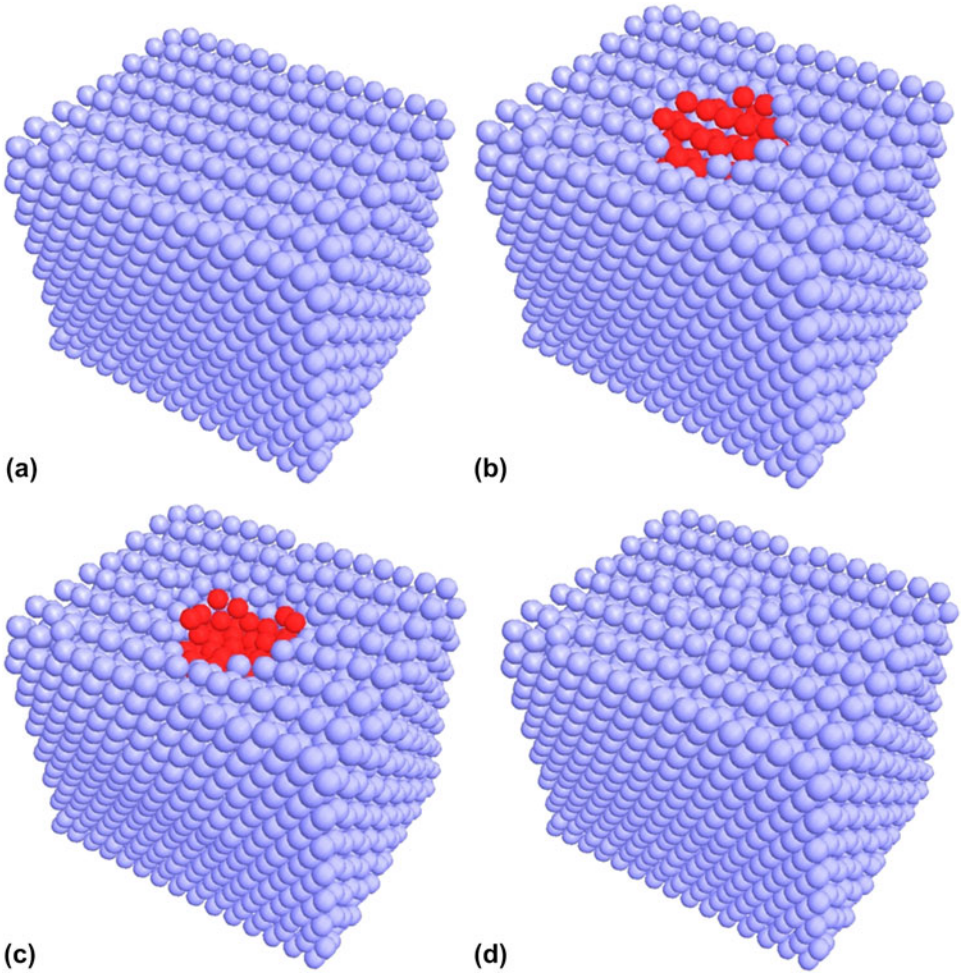

FIG. 2. Visualization of a material used in simulations: (a) after equilibration but before indentation, (b) at the first force iteration, (c) at the last force iteration, and (d) after a 60-simulation step postindentation recovery period (≈600 ns).

a separate simulation that is averaged over three materials. A data point corresponds to the average vertical position of a group of segments, averaged over three materials, under the indenter for successive simulation steps, and the lines that connect each data point show the profile of indentation depth and recovery. Segments tend to shift downward under the influence of the indenter and recover over time once the applied force is removed. Intuitively, as the external force increases, the indenter penetrates the material deeper, as seen in Fig. 3. These facts provide a validation[44] of our model. For a constant indenter size, larger forces tend to affect recovery significantly. We note that, for a given applied force, smaller indenter size means a larger force applied per unit surface area. Therefore, for the largest force (147-nm indenter surface area), we have the largest depth around 250 nm, for the 245-nm indenter that depth is below 130 nm, whereas for the 343 nm indenter, the respective depth is 56 nm.

Figure 4 provides a different view, namely the effect of changing the indenter diameter under a constant force. Each curve corresponds to a group of segments subject to the indenter, previously shown in Fig. 2 as the highlighted red segments. The curve for the smallest indenter in Fig. 4(a) features the deepest indentation within the tested range. The material is indented to a penetration depth $R_p = 20.4$ nm and recovers to a depth $R_h = 1.4$ nm. Thus, the corresponding φ from Eq. (1) is 93%.

Figure 5 shows the top view of a material that is being indented with a small and a large indenter. Essentially, a wider indenter means that there are more chain segments collectively resisting indentation.

R_p curves as a function of external force are shown in Fig. 6. For constant indenter size, each curve shows that, as the force increases, R_p increases in magnitude. As expected from the above results presented with different coordinates, small indenters penetrate the material deeper than large indenters. We see that the range of R_p for large indenters is narrower than for small indenters.

Figure 7 shows the residual depth R_h. Also here when the external force per unit surface area increases (smaller indenter diameter), R_h increases. The resulting recovery

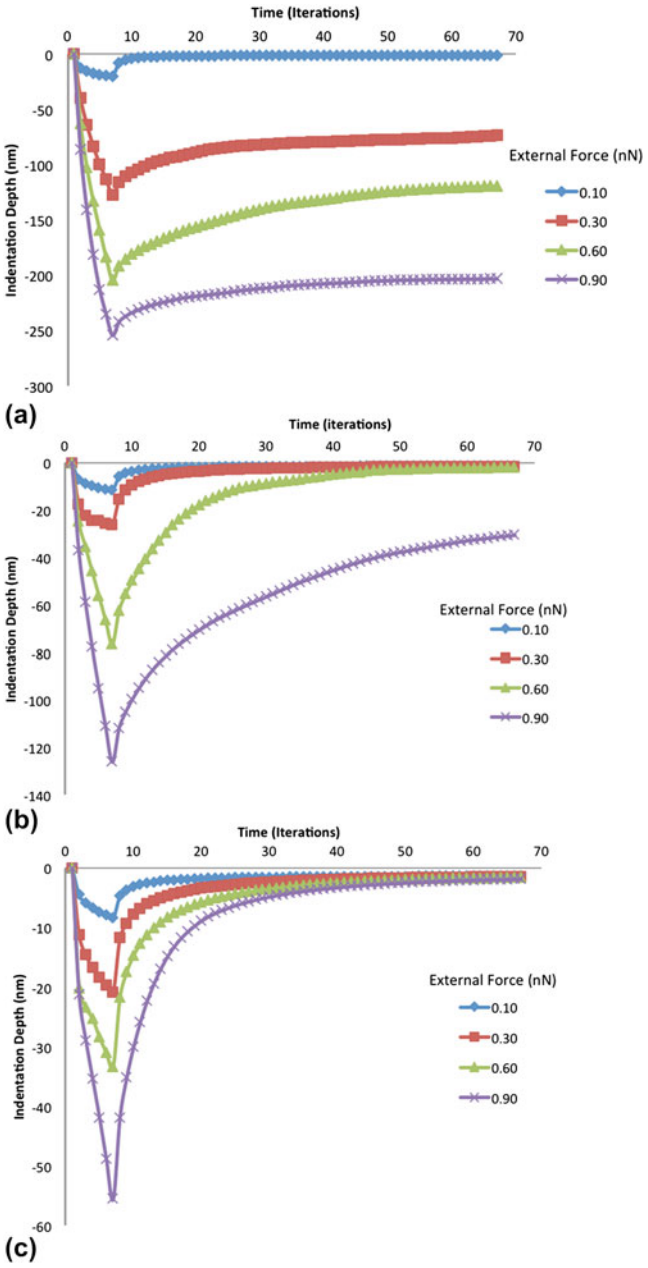

FIG. 3. The indentation depth as a function of time for different external forces with indenter diameters (a) 147 nm, (b) 245 nm, and (c) 343 nm. Data points represent vertical positions of the group of segments under the indenter at each time iteration. The lines that connect each data point show penetration and recovery trends. Segments tend to shift down as a result of the applied force and recover over time. The external force was applied for six simulation steps.

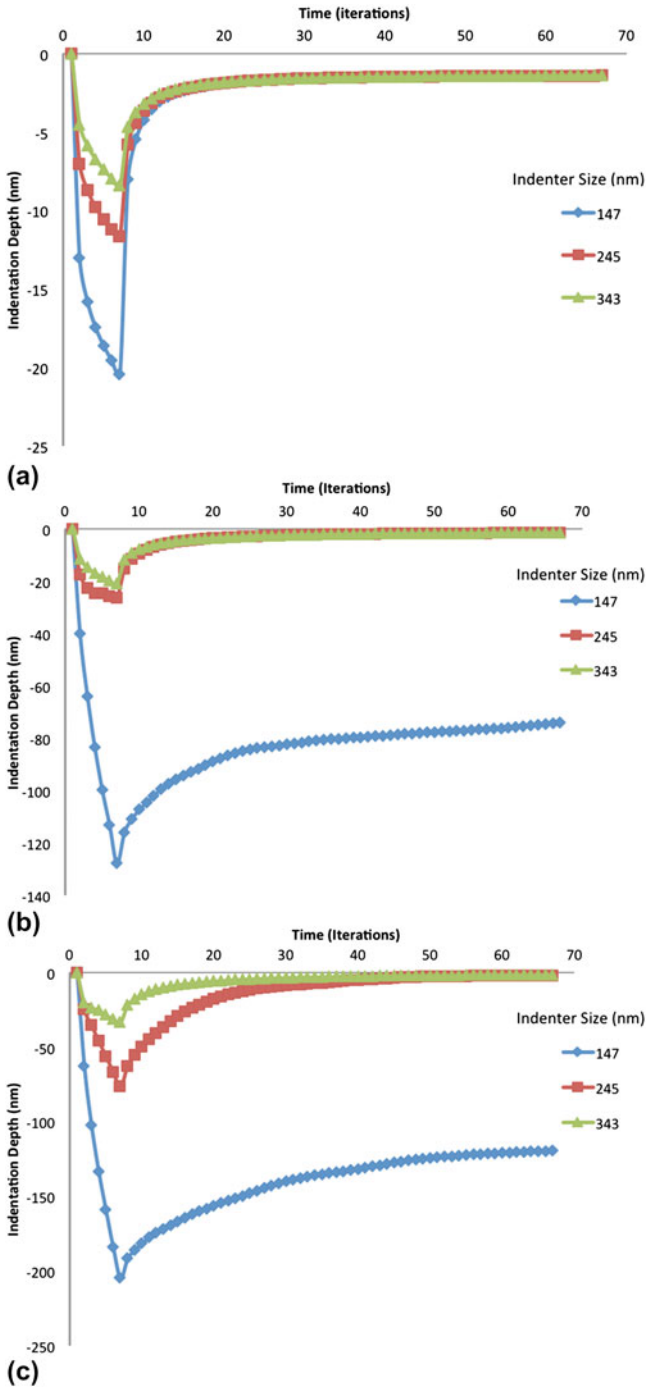

FIG. 4. The indentation depth as a function of time for different indenter sizes at (a) 0.10 nN, (b) 0.30 nN, and (c) 0.60 nN. The external force was applied for six simulation steps. The number of indented segments naturally increases as the indenter diameter increases (at a rate proportional to the radius squared). As a result, there is a significant reduction in the magnitude of the penetration depth for larger indenters because the external force is divided uniformly for each segment under the indenter.

percentage is shown in Fig. 8. For different indenter sizes, φ drops off at different force levels (0.10, 0.50, and 1.0 nN). Again, as the larger indenter distributes the force over more segments, it applies a much smaller force per segment. The result is a higher φ value for large indenters.

We next analyze the indentation results in an alternative way: penetration and recovery depths as functions of indenter diameter for constant external force levels. Results for R_p, R_h, and φ are shown in Figs. 9–11 respectively. Figures 9–11 confirm the conclusions above; for a given

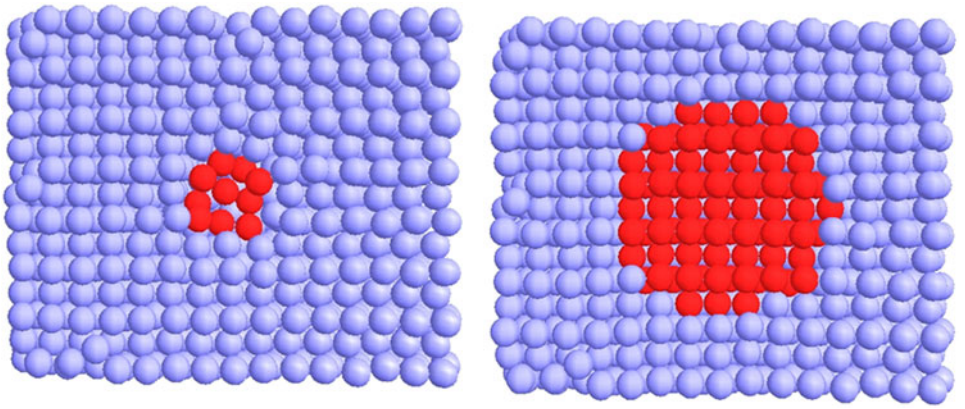

FIG. 5. Top view of a small (147-nm diameter) and large (343-nm diameter) indenter applying an external force on a 600 × 600 × 600 nm segmented material.

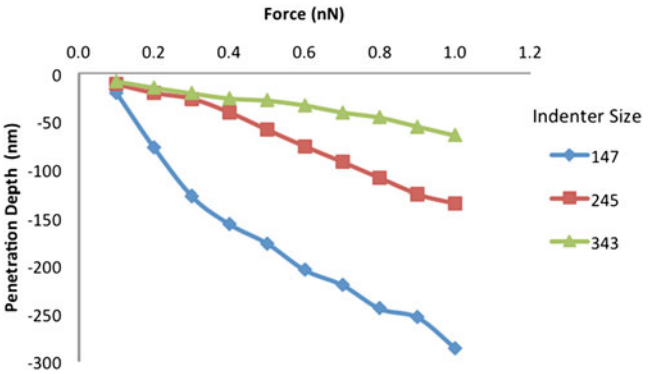

FIG. 6. R_p as a function of the applied external force for three materials with three different indenter sizes.

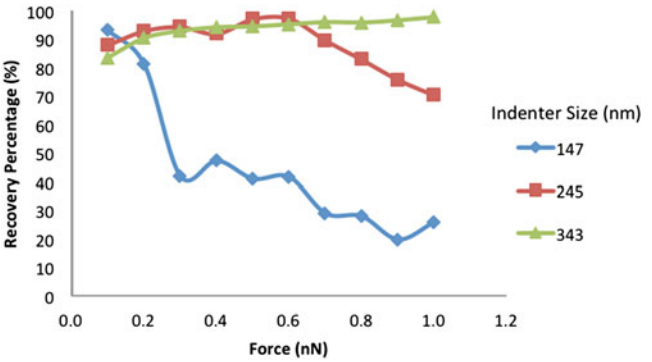

FIG. 8. Recovery percentage φ as a function of the applied external force.

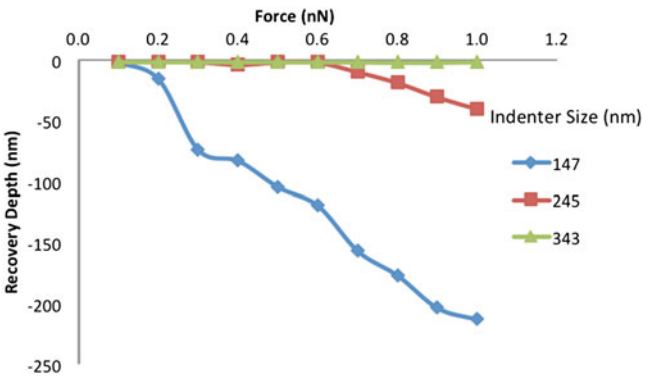

FIG. 7. R_h as a function of the applied external force.

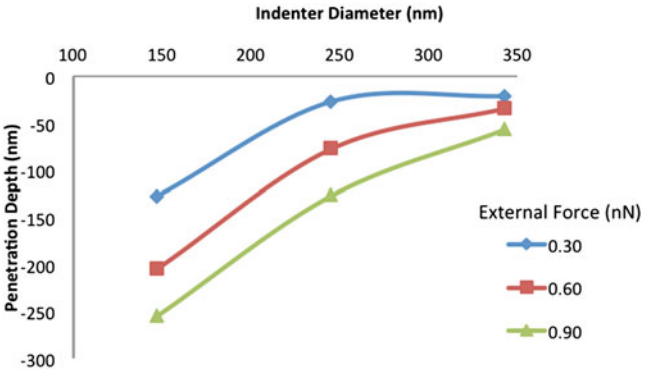

FIG. 9. R_p as a function of the indenter diameter.

external force, samples which were indented with a larger indenter exhibit shallower recovery depths, and increasing indenter size yields higher φ values.

B. Time of application of the force

For the entirety of the previous section, the time that the external force was applied was held constant at 60 ns (6 simulation steps). We now report the effects of the time variation on the indentation and recovery depths for varying force levels at a constant indenter size.

Figure 12 shows a series of plots for the indentation depth for different times during which the external force was applied.

For a given force level, we see that as the number of force steps increases, the indenter penetrates deeper into the material. This constitutes one more validation of our model. We also see that, as the indenter penetrates deeper

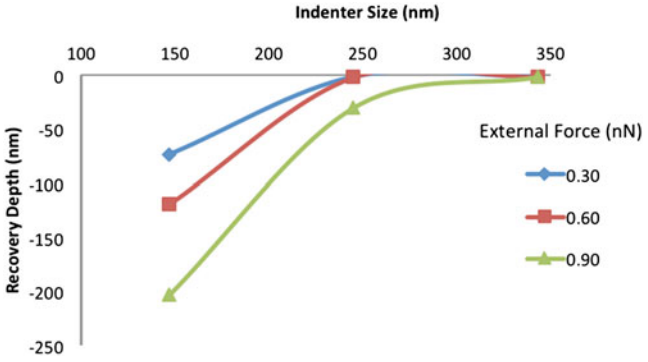

FIG. 10. R_h as a function of the indenter diameter.

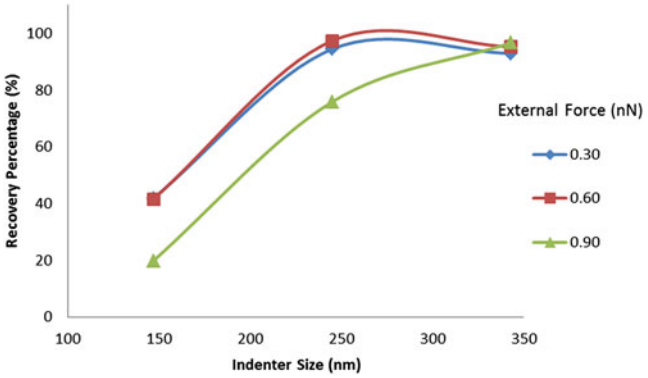

FIG. 11. Recovery percentage φ as a function of the indenter diameter.

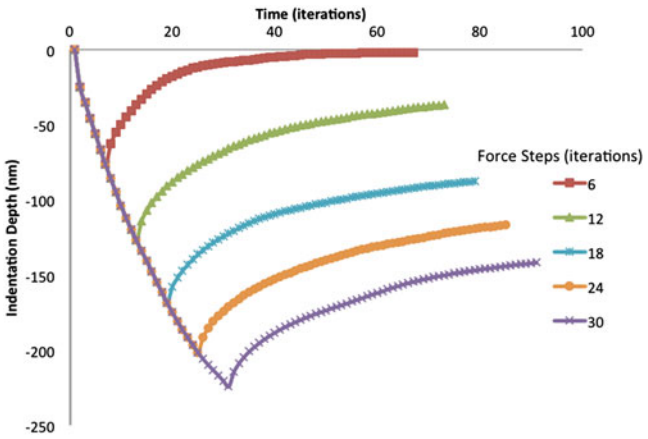

FIG. 12. The indentation depth as a function of time iterations with a 245-nm diameter indenter for 0.60-nN applied external force. Each plot represents constant conditions (indenter size, applied force, and the same material) with each curve corresponding to a different time frame for application of the indentation force. The time of reaching a plateau as a function of the time of the force imposition is seen.

into the material, there is overall a higher collective resistance to indentation.

There is also a significant shift in behavior from 0.30 to 0.60 nN. This indicates that additional deformation

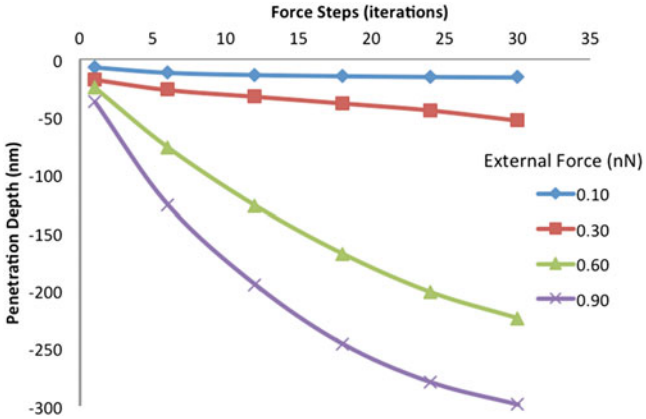

FIG. 13. R_p as a function of force steps for 0.10, 0.30, 0.60, and 0.90 nN. As expected, for a given indenter diameter, as the number of force steps increases, the magnitude of the penetration depth increases.

mechanisms are enabled at that point, and allow deeper penetrations. In fact, we have verified that the number of broken bonds increases in simulations at higher force levels; thus, the mechanism of chain scission is enabled for higher applied indenter force levels.

R_p is shown in Fig. 13 from 0.10 to 0.90 nN. As time increases, the depth displays "diminishing returns." That is, each force step does not penetrate as deeply as the previous one.

Figure 14 shows the recovery percentage as a function of the number of force steps during which the indentation force is applied. External forces of 0.10 and 0.30 nN exhibit a high φ, independent of how long the force is applied (even if the penetration depth slightly increases along time). As expected, large forces result in lower recovery.

C. Combined effect of force and time

Due to a similar effect that was observed from the indentation force and indentation time parameters, a further analysis was conducted. To counterbalance these two parameters, they were varied in a way that the product between the indentation force and the indentation time is held constant at 0.90 nN × ps. The concept behind this study is to observe how the material behaves if a smaller force is applied for a longer time interval or a larger force applied for a shorter time interval. The results are shown in Fig. 15. As expected, higher forces penetrate deeper into the material even if applied for a much shorter interval. Even if a lower force is applied for much longer time, it will not produce the same penetration depth as a higher force in a short interval. Clearly, different deformation mechanisms are available at different force levels. Nevertheless, it should be noted that the recovery percentages are very similar for all studied cases (and exhibit an average value of 93.73% ± 0.03).

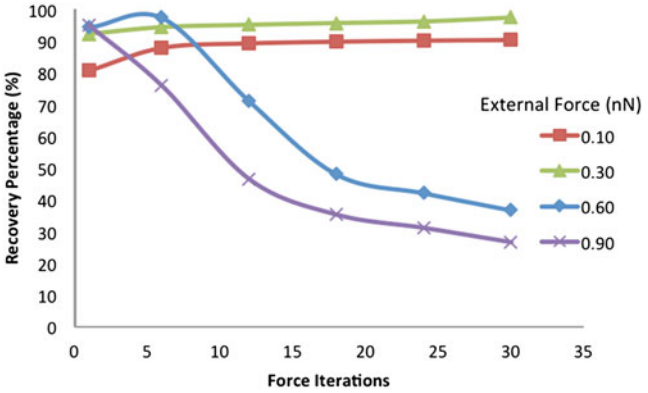

FIG. 14. The recovery percentage φ as a function of force steps for 0.10, 0.30, 0.60, and 0.90 nN. As the number of force steps increases, large forces produce low φ values, whereas for low forces, the recovery remains high.

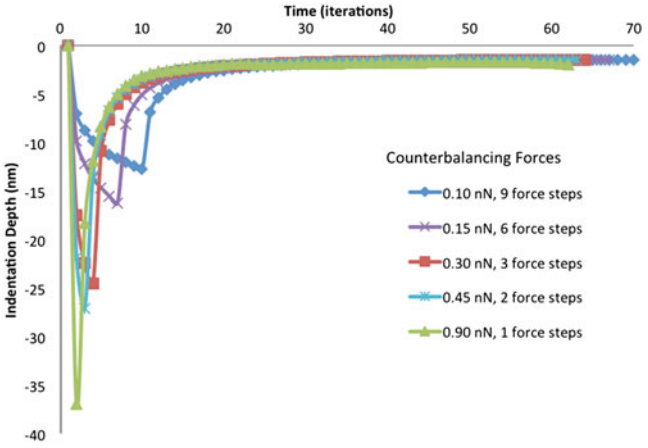

FIG. 15. Indentation depth as a function of indentation force and indentation time. For constant products between the force and the number of force steps (0.90 nN × ps), each curve shows a similar recovery behavior.

IV. CONCLUDING REMARKS

We have used computer simulations to study the indentation behavior of an HDPE polymer model through MD. Although, as a first approach, the used computer model considers only a few parameters, it can be expanded in the future, such as incorporating a second phase or controlling the degree of chain orientation.

From the present indentation results, we have shown that (i) an increasing external force results in an increase in the indentation depth and decrease in the viscoelastic recovery φ; (ii) a larger indenter size, under constant external force, results in decreasing the depth and increasing φ; (iii) increasing the amount of time that the indenter is applied increases the depth and may reduce φ for higher force levels; and (iv) the force level and time during which the force is applied are not entirely interchangeable, and appear to be associated with different deformation mechanisms—even though they always recover to a similar φ.

The indentation behavior observed from simulations provides valuable insights into the mechanisms through which tribological properties are defined for the material. Overall, simulations provide complementary information to that of experiments and provide much more details into specific localized phenomena that take place in the material—phenomena unavailable experimentally. In experiments, it is impossible to track the response of individual polymer chains. It is not possible experimentally to apply different forces at exactly the same location in the same material. By developing an improved understanding of ways to obtain the desired material properties, we reduce effort and time spent on experiments of the trial-and-error type.

We are dealing with simple one-phase carbonic chains. There are computer simulations of more complicated polymeric materials, notably work of the Stockholm school on polyethylene including spherulites, using MD as well as off-lattice Monte Carlo techniques.[45–50]

Finally, let us point out the instructional value of our simulations. There is a growing emphasis in teaching Materials Science and Engineering on atomic, molecular, and nano-levels.[51–60] Visualizations obtained from our simulation results are also helpful in this respect.

ACKNOWLEDGMENTS

Partial financial support has been provided by the Foundation for Science and Technology (FCT), Lisbon, through Grant Nos. PEst-C/CTM/LA0025/2013 and PTDC-EME-PME-108859-2008, and also by the II-VI Foundation, Bridgeville, Pennsylvania. The late Rustum Roy has taught us how to do *integration* of science and engineering and how to avoid even unintentional fragmentation of science.

REFERENCES

1. J. Suwanprateeb: A comparison of different methods in determining load- and time-dependence of Vickers hardness in polymers. *Polym. Test.* **17**, 495 (1998).
2. E. Amitay-Sadovsky and H.D. Wagner: Evaluation of Young's modulus of polymers from Knoop microindentation tests. *Polymer* **39**, 2387 (1998).
3. L. Anand and N.M. Ames: On modeling the micro-indentation response of an amorphous polymer. *Int. J. Plast.* **22**, 1123 (2006).
4. Y.C. Lu and D.M. Shinozaki: Effects of substrate constraint on micro-indentation testing of polymer coatings. *Mater. Sci. Eng.* **396**, 77 (2005).
5. X. Li and B. Bhushan: A review of nanoindentation continuous stiffness measurement technique and its applications. *Mater. Charact.* **48**, 11 (2002).
6. S. Pathak, J.G. Swadener, S.R. Kalidindi, H.W. Courtland, K.J. Jepsen, and H.M. Goldman: Measuring the dynamic mechanical response of hydrated mouse bone by nanoindentation. *J. Mech. Behav. Biomed. Mater.* **4**, 34 (2011).

7. D. Li, Y-W. Chung, M-S. Wong, and W.D. Sproul: Nano-indentation studies of ultrahigh strength carbon nitride thin films. *J. Appl. Phys.* **74**, 219 (1993).
8. Y-G. Jung, B.R. Lawn, M. Martyniuk, H. Huang, and X.Z. Hu: Evaluation of elastic modulus and hardness of thin films by nanoindentation. *J. Mater. Res.* **19**, 3076 (2004).
9. S. Suresh, T-G. Nieh, and B.W. Choi: Nanoindentation of copper thin films on silicon substrates. *Scr. Mater.* **41**, 951 (1999).
10. G.M. Odegard, T.S. Gates, and H.M. Herring: Characterization of viscoelastic properties of polymeric materials through nanoindentation. *Exp. Mech.* **45**, 130 (2005).
11. S.P. Ho, L. Riester, M. Drews, T. Boland, and M. LaBerge: Nanoindentation properties of compression-moulded ultra-high molecular weight polyethylene. *Proc. Inst. Mech. Eng. Part H J. Eng. Med.* **217**, 357 (2003).
12. C. Klapperich, K. Komvopoulos, and L. Pruitt: Nanomechanical properties of polymers determined from nanoindentation experiments. *ASME* **123**, 624 (2001).
13. K. Park, S. Mishra, G. Lewis, J. Losby, Z. Fan, and J.B. Park: Quasi-static and dynamic nanoindentation studies on highly crosslinked ultra-high-molecular-weight polyethylene. *Biomaterials* **25**, 2427 (2004).
14. M. Bischel, M.R. Vanlandingham, R.F. Eduljee, J.W. Gillespie, and J.M. Schultz: On the use of nanoscale indentation with the AFM in the identification of phases in blends of linear low density polyethylene and high density polyethylene. *J. Mater. Sci.* **35**, 221 (2000).
15. S. Fossey: Computer simulation of mechanical properties, in *Performance of Plastics*, edited by W. Brostow (Hanser, Munich, Cincinnati, 2000).
16. F. Cleymand, O. Ferry, R. Kouitat, A. Billard, and J. von Stebut: Influence of indentation depth on the determination of the apparent Young's modulus of bi-layer material: Experiments and numerical simulation. *Surf. Coat. Technol.* **200**, 890 (2005).
17. B.J. Alder and T.E. Wainwright: Studies in molecular dynamics. I. General method. *J. Chem. Phys.* **31**, 459 (1959).
18. T. Yamamoto: Molecular dynamics modeling of polymer crystallization from the melt. *Polymer* **45**, 1357 (2004).
19. K. Yashiro, A. Furuta, and Y. Tomita: Molecular dynamics simulation of polyethylene under cyclic loading: Effect of loading condition and chain length. *Int. J. Mech. Sci.* **52**, 136 (2010).
20. S. Blonski, W. Brostow, and J. Kubat: Molecular-dynamics simulations of stress relaxation in metals and polymers. *Phys. Rev. B* **49**, 6494 (1994).
21. A.F. Terzis and E. Paspalakis: *Recent Research Topics and Developments in Chemical Physics: From Quantum Scale to Macroscale* (Transworld Research Network, Kerala, India, 2008).
22. K. Binder: *Monte Carlo, and Molecular Dynamics Simulations in Polymer Sciences* (Oxford University Press, Oxford, UK, 1995).
23. M. Kotelyanskii and D.N. Theodorou: *Simulation Methods for Polymers* (Marcel Dekker, New York, 2004).
24. W. Brostow and R. Simoes: Tribological behavior of polymers simulated by molecular dynamics. *J. Mater. Res.* **27**, 851 (2005).
25. T. Hilbig, W. Brostow, and R. Simoes: Simulating scratch behavior of polymers with mesoscopic molecular dynamics. *Mater. Chem. Phys.* **139**, 118 (2013).
26. W. Brostow, M. Donahue, C.E. Karashin, and R. Simoes: Graphical modeling and computer animation of tensile deformation in polymer liquid crystals (PLCs). *Mater. Res. Innovat.* **4**, 75 (2001).
27. S.J.V. Frankland, V.M. Harik, G.M. Odegard, D.W. Brenner, and T.S. Gates: The stress-strain behavior of polymer-nanotube composites from molecular dynamics simulation. *Compos. Sci. Technol.* **63**, 1655 (2003).
28. R. Komanduri, N. Chandrasekaran, and L.M. Raff: Effect of tool geometry in nanometric cutting: A molecular dynamics simulation approach. *Wear* **219**, 84 (1998).
29. R. Komanduri and N. Chandrasekaran: Molecular dynamics simulation of atomic-scale friction. *Phys. Rev. B* **61**, 14007 (2000).
30. R. Komanduri, N. Chandrasekaran, and L.M. Raff: MD simulation of indentation and scratching of single crystal aluminum. *Wear* **240**, 113 (2000).
31. W.C.D. Cheong and L.C. Zhang: Molecular dynamics simulation of phase transformation in silicon monocrystals due to nano-indentation. *Nanotechnology* **11**, 173 (2000).
32. X-L. Ma and W. Yang: Supersonic wave propagation in Cu under high speed cluster impact. *Nanotechnology* **15**, 449 (2004).
33. L. Zhang and H. Tanaka: On the mechanics and physics in the nano-indentation of silicon monocrystals. *JSME Int J., Ser. A* **42**, 546 (1999).
34. W.G. Hoover, A.J. de Groot, C.G. Hoover, I.F. Stowers, T. Kawai, B.L. Holian, T. Boku, S. Ihara, and J. Belak: Large-scale elastic-plastic indentation simulations via nonequilibrium molecular dynamics. *Phys. Rev.* **42**, 5844 (1990).
35. C. Luo and J-U. Sommer: Coding coarse grained polymer model for LAMMPS and its application to polymer crystallization. *Comput. Phys. Commun.* **180**, 1382 (2009).
36. J. Baschnagel, K. Binder, P. Doruker, A. Gusev, O. Hahn, K. Kremer, W. Mattice, F. Muller-Plathe, M. Murat, W. Paul, S. Santos, U.W. Suter, and V. Tries: Bridging the gap between atomistic and coarse-grained models of polymers: Status and perspectives, *Adv. Polym. Sci.* **152**, 41 (2000).
37. W. Brostow, J.A. Hinze, and R. Simoes: Tribological behavior polymers simulated by molecular dynamics. *J. Mater. Res.* **19**, 851 (2004).
38. W. Brostow, S. Deshpande, T. Hilbig, and R. Simoes: Molecular dynamics computer simulation of scratch resistance testing of polymers: Visualization. *Polym. Bull.* **70**, 1457 (2013).
39. W. Brostow, A.M. Cunha, and R. Simoes: Generation of polymeric structures on a computer. *Mater. Res. Innovat.* **7**, 19 (2003).
40. W. Brostow, J-L. Deborde, M. Jaklewicz, and P. Olszynski: Tribology with emphasis on polymers: Friction, scratch resistance and wear. *J. Mater. Educ.* **25**, 119 (2003).
41. W. Brostow, V. Kovacevic, D. Vrsaljko, and J. Whitworth: Tribology of polymers and polymer-based composites. *J. Mater. Educ.* **32**, 273 (2010).
42. B.D. Beake, G.A. Bell, W. Brostow, and W. Chonkaew: Nanoindentation creep and glass transition temperatures in polymers. *Polym. Int.* **56**, 773 (2007).
43. W. Brostow, W. Chonkaew, R. Mirshams, and A. Srivastava: Characterization of grooves in scratch resistance testing. *Polym. Eng. Sci.* **48**, 2060 (2008).
44. P. Bratley, B.L. Fox, and L.E. Schrage, *A Guide to Simulation*, 2nd ed. (Springer Verlag, Berlin, Heidelberg, New York, 1987).
45. A. Matozza, P. Serralunga, M.S. Hedenqvist, and U.W. Gedde: Mesoscale modelling of penetrant diffusion in computer-generated polyethylene-spherulite-like structures. *Polymer* **47**, 5588 (2006).
46. J. Ritums, B. Neway, F. Doghieri, G. Bergman, U.W. Gedde, and M.S. Hedenqvist: Assessing the transport properties of organic penetrants in low-density polyethylene using a "four-component" polymer free-volume model and a comparison with a semi empirical exponential model. *J. Polym. Sci. Phys.* **45**, 723 (2007).
47. A. Matozzi, M. Minelli, M.S. Hedenqvist, and U.W. Gedde: Computer-built polyethylene spherulites for mesoscopic Monte Carlo simulation of penetrant diffusion: Influence of crystal widening and thickening. *Polymer* **48**, 2453 (2007).
48. A. Matozzi, M.S. Hedenqvist, and U.W. Gedde: Diffusivity of n-hexane in poly(ethylene-co-octene)s assessed by molecular dynamics simulations. *Polymer* **48**, 5174 (2007).
49. F. Nilsson, U.W. Gedde, and M.S. Hedenqvist: Penetrant diffusion in polyethylene spherulites assessed by a novel off-lattice Monte-Carlo technique. *Eur. Polym. J.* **45**, 3409 (2009).

50. F. Nilsson, X. Lan, T. Gkourmpis, M.S. Hedenqvist, and U.W. Gedde: Modeling tie chains and trapped entanglements in polyethylene. *Polymer* **53**, 3594 (2012).
51. E. Goo: The structure of matter: A science literacy course at USC. *J. Mater. Educ.* **24**, 203 (2002).
52. K.L. Miller and C.C. Wamser: Materials science for the non-science major. *J. Mater. Educ.* **25**, 189 (2003).
53. D. Roylance: A new MSE curriculum. *J. Mater. Educ.* **26**, 233 (2004).
54. L. Vanasupa and L.G. Splitt: Curricula for a sustainable future: A proposal for integrating environmental concepts into our curricula. *J. Mater. Educ.* **26**, 293 (2004).
55. M. Meyyappan: Nanotechnology education and training. *J. Mater. Educ.* **26**, 313 (2004).
56. H.E. Hagg Lobland: Strange matter: Student impressions of a museum exhibit by the Materials Research Society. *J. Mater. Educ.* **27**, 29 (2005).
57. L.C. Klein: Implementing an undergraduate interdisciplinary concentration in nanomaterials science and engineering. *J. Mater. Educ.* **28**, 7 (2006).
58. D-B. Shieh, C-S. Yeh, W-C. Chang, and Y. Tzeng: The integration of biomedical nanotechnology education program in Taiwan. *J. Mater. Educ.* **29**, 107 (2007).
59. N. Skoulidis and H.M. Polatoglou: Integrated tool for the teaching of structural and optical properties of nanostructures. *J. Mater. Educ.* **29**, 117 (2007).
60. M. Hess: Integration of materials science in the education of high school teachers in an advanced course program. *J. Mater. Educ.* **33**, 141 (2011).